Discrete-Time Modeling and Control Based on Field Orientation for Induction Motors

Jorge Rivera Domínguez, Iván Dueñas, and Susana Ortega-Cisneros

***Abstract*—In this article, discrete-time direct and indirect field-oriented controllers (FOCs) for induction motors (IMs) are designed. Based on a discrete-time stationary reference frame model for IMs, which was obtained by means of a variational integrator, the stationary model is oriented to the field. Then, discrete-time FOCs, in the direct and indirect versions, are designed for tracking of reference signals for the rotor velocity and the rotor flux modulus. A simulation study was carried out, and for comparison purposes, discretized continuous-time FOCs were also simulated for three sampling periods. It was put in evidence that the proposed discrete-time controllers performed better than the discretized counterparts when the sampling period was increased. Real-time experiments were carried out for discrete-time direct and indirect FOCs, where their performances were similar to those predicted by simulations.**

***Index Terms*—Digital control, discrete-time systems, induction motors (IMs).**

NOMENCLATURE

IM variables

Rotor velocity	ω_k [rad/s].
Electromagnetic torque	$\tau_{e,k}$ [N·m].
Load torque	$\tau_{L,k}$ [N·m].
Rotor flux vector	$\Phi_{d,q,k} = (\phi_{d,k}, \phi_{q,k})^T$ [Wb].
Rotor flux modulus	$\phi_{d,k}$ [Wb].
Stator current vector	$I_{d,q,k} = (i_{d,k}, i_{q,k})^T$ [A].
Input voltage vector	$U_{d,q,k} = (u_{d,k}, u_{q,k})^T$ [V].
Slip angular velocity	$\omega_{s,k}$ [rad/s].
Synchronous velocity	$\omega_{\phi,k}$ [rad/s].

User-defined variables for IMs

$\eta_{2,k}$	$1/(\tau_{r,d}\cos(T_s\omega_{s,k}))$.
$\eta_{3,k}$	$T_sL_m\eta_{2,k}/\tau_r$ [H].
$\varphi_1(x,y,z)$	$\cos(T_sx)y + \sin(T_sx)z$.
$\varphi_2(x,y,z)$	$-\sin(T_sx)y + \cos(T_sx)z$.
$\psi_{d,k}$	$\phi_{d,k} + \frac{T_sL_m}{\tau_r}i_{d,k}$.
$\psi_{q,k}$	$\phi_{q,k} + \frac{T_sL_m}{\tau_r}i_{q,k}$.

IM parameters

Stator resistance	$R_s = 1.115$ [Ω].
Rotor resistance	$R_r = 1.083$ [Ω].
Stator inductance	$L_s = 209.7 \times 10^{-3}$ [H].
Rotor inductance	$L_r = 209.7 \times 10^{-3}$ [H].
Mutual inductance	$L_m = 203.7 \times 10^{-3}$ [H].
Inertia moment	$J = 0.02$ [kg·m^2].
Number of pole pairs	$p = 2$
Sampling period	$T_s = \{0.1, 0.6, 3\} \times 10^{-3}$ [s].

User-defined constants for IMs

Torque constant (k_T)	$3pL_m/(2L_r) = 2.7398$.
Rotor time constant (τ_r)	$L_r/R_r = 0.0408$ [s].
σ	$L_s - L_m^2/L_r = 5.5695\times^{-2}$ [H].
β	$L_m/(\sigma L_r) = 16.398$ [1/H].
γ	$(R_s + L_m^2R_r/L_r^2)/\sigma = 402.62$ Ω/H].
$\tau_{r,d}$	$1 + T_s/\tau_r$.
σ_d	$\sigma + T_sL_m^2/(L_r\tau_r\tau_{r,d}^2)$ [H].
β_d	$L_m/(L_r\sigma_d)$ [1/H].
γ_d	$1 - R_sT_s/\sigma_d$.
η_1	$\tau_{r,d}/k_T$.
η_2	$1/\tau_{r,d}$.
η_3	$T_sL_m\eta_2/\tau_r$ [H].
$\mathcal{J}$	$\begin{pmatrix} 0 & -1 \\ 1 & 0 \end{pmatrix}$.
a_1	$(\gamma_d - k_{11} + \eta_2)$.
a_2	$(k_{11}\eta_2/\eta_3 - \eta_2^2/\eta_3 + k_{12}T_s/\eta_3)$.
a_3	$T_sk_T\phi_{d,r,k}/(J\tau_{r,d})$.
a_4	$(\gamma_d + 1 - k_{31})$.
a_5	$(1/a_3 - k_{31}/a_3 - k_{32}T_s/a_3)$.

DTFOC

Rotor velocity reference signal	$\omega_{r,k}$ [rad/s].
Rotor flux modulus reference signal	$\phi_{d,r,k}$ [Wb].
d current reference signal	$i_{d,r,k}$ [A].

Manuscript received June 6, 2019; revised October 21, 2019; accepted December 25, 2019. Date of publication January 9, 2020; date of current version April 22, 2020. Recommended for publication by Associate Editor G. Escobar. *(Corresponding author: Jorge Rivera Domínguez.)*

J. R. Domínguez is with the CONACyT–CINVESTAV del IPN, 45010 Zapopan, México (e-mail: riveraj@gdl.cinvestav.mx).

I. Dueñas and S. Ortega-Cisneros are with the CINVESTAV del IPN, 45010 Zapopan, México (e-mail: ivan_iedg@hotmail.com; sortega@gdl.cinvestav.mx).

Color versions of one or more of the figures in this article are available online at https://ieeexplore.ieee.org.

Digital Object Identifier 10.1109/TPEL.2020.2965632

q current reference signal — $i_{q,r,k}$ [A].
Pseudo-control input vector — $V_{d,q,k} = (v_{d,k}, v_{q,k})^T$ [A].

DTDFOC

Rotor flux mod. tracking error — $\chi_{d,k} = \phi_{d,k} - \phi_{d,r,k}$ [Wb].
d current tracking error — $e_{id,k} = i_{d,k} - i_{d,r,k}$ [A].
Unknown constant term — $\delta_{d,k} = \frac{k_{12}T_s}{\eta_3}\phi_{d,r,k} + \frac{k_{11}+1}{\eta_3}\phi_{d,r,k+1}$.
Integral of $\chi_{d,k}$ — $\bar{g}_{d,k} = \sum_{n=1}^{k} T_s\chi_{d,n-1}$ [s·Wb].
Integral of $e_{id,k}$ — $g_{d,k} = \sum_{n=1}^{k} T_s e_{id,n-1}$ [s·A].
Rotor velocity tracking error — $\chi_{q,k} = \omega_k - \omega_{r,k}$ [rad/s].
q current tracking error — $e_{iq,k} = i_{q,k} - i_{q,r,k}$ [A].
Unknown constant term — $\delta_{q,k} = \frac{(k_{31}-a_3)T_s\tau_{L,k}}{Ja_3} + \frac{(k_{32}T_s-k_{31})\omega_{r,k}}{a_3}$.
Integral of $\chi_{q,k}$ — $\bar{g}_{q,k} = \sum_{n=1}^{k} T_s\chi_{q,n-1}$ [rad].
Integral of $e_{iq,k}$ — $g_{q,k} = \sum_{n=1}^{k} T_s e_{iq,n-1}$ [s·A].
Estimated rotor flux vector — $\hat{\Phi}_{r,k} = (\hat{\phi}_{\alpha,r,k}, \hat{\phi}_{\beta,r,k})^T$ [Wb^2].
Estimated rotor flux angle — $\hat{\theta}_{\phi,k}$ [rad].
Proportional gains — $k_{11}, k_{21}, k_{31}, k_{41}$.
Integral gains — $k_{12}, k_{22}, k_{32}, k_{42}$.

DTIFOC

Rotor flux mod. tracking error — $e_{\phi,k} = \phi_{d,k} - \phi_{d,r,k}$ [Wb].
d current tracking error — $\varepsilon_{d,k} = i_{d,k} - i_{d,r,k}$ [A].
Integral of $\varepsilon_{d,k}$ — $\zeta_{d,k} = \sum_{n=1}^{k} T_s\varepsilon_{d,n-1}$ [s·A].
Unknown constant term — $\rho_{d,k} = (\gamma_d - 1)(1 - \eta_2)\phi_{d,r,k}/\eta_3$.
Rotor velocity tracking error — $e_{\omega,k} = \omega_k - \omega_{r,k}$ [rad/s].
q current tracking error — $\varepsilon_{q,k} = i_{q,k} - i_{q,r,k}$ [A].
Integral of $e_{\omega,k}$ — $g_k = \sum_{n=1}^{k} T_s e_{\omega,n-1}$ [rad].
Integral of $\varepsilon_{q,k}$ — $\zeta_{q,k} \sum_{n=1}^{k} T_s\varepsilon_{q,n-1}$ [s·A].
Unknown constant term — $\rho_{q,k} = \gamma_d i_{q,r,k} - i_{q,r,k+1}$.
Required slip angular velocity — $\omega_{s,r,k}$ [rad/s].
Rotor flux angle — $\theta_{\phi,k}$ [rad].
Proportional gains — $\kappa_{11}, \kappa_{21}, \kappa_{31}$.
Integral gains — $\kappa_{12}, \kappa_{22}, \kappa_{32}$.

Acronyms

DTFOC — Discrete-time field-oriented control.
DTM — Discrete-time model.
DTDFOC — Discrete-time direct field-oriented control.
DTIFOC — Discrete-time indirect field-oriented control.
DSP — Digital signal processor.
FOC — Field-oriented control.
FPGA — Field-programmable gate array.
IM — Induction motor.
RHONN — Recurrent high-order neural network.
SEM — Symplectic Euler method.
SDFOC — Sampled direct field-oriented control.
SIFOC — Sampled indirect field-oriented control.

I. Introduction

FIVE decades ago, the pioneering work of Blaschke [1] introduced a novel control technique for the IM [2], [3] known as FOC. This technique relies on a nonlinear transformation and feedback that make the decoupling between the outputs and the control inputs feasible. In fact, the IM mathematical model resembles to that of a dc motor with separated excitation [4]. Since then, the research community has been inspired by the FOC technique, where important improvements have been made by combining FOC with modern control approaches as just reported in the literature, for example, with backstepping [5], input–output linearization [6], [7], sliding modes [8], [9], passivity [10], fuzzy logic [11], [12], and direct torque control [13], among others. It is worth mentioning that these works are designed in a continuous-time setting and implemented with digital devices.

There are two options for designing a control algorithm with its corresponding implementation in digital devices. The first option consists of designing the controller in a continuous-time setting and then discretizing it by means of the explicit Euler method. This option works fine for high sampling rates or for systems with slow dynamics [14]. In the case of a custom hardware design of the algorithm as for very large scale integration or FPGA devices [15], this option will demand digital devices with high clock frequencies yielding in a relatively large power consumption, increasing the cost of the digital implementation [16]. The second option deals with the sampling of the dynamics of the continuous-time system and with the design of a discrete-time controller that can be directly implemented in any digital device. The advantage of this option is that the sampling period can significantly be increased if the accuracy of the sampled model is high. The accuracy due to sampling is guaranteed to be exact for linear systems, but for nonlinear systems, it is a difficult task [17].

With respect to DTFOC, researchers have made some advances as reported in [18], where an exact DTM of a current-fed (reduced-order model) IM was presented and used for designing a DTFOC controller. Based on a DTM obtained by means of the

explicit Euler method, DTFOCs were designed in [19] and [20], where high sampling rates are required. Moreover, in [20], Gao's discrete-time reaching law was used, which employs a sign function causing chattering problems. In [21], the reference stator currents were designed in continuous time, whereas the stator current dynamics were approximated in discrete time for an FOC law design. A sensorless DTFOC was designed in [22], where the explicit Euler method was used under the assumption of constant rotor velocity, along with the employment of a sign function in the control design. In [23], a discrete-time neural inverse optimal control based on an RHONN is presented. Although the RHONN is an identifier for obtaining an accurate IM model, the general proposal relies on rotor flux estimations that are based on a model approximated by means of the explicit Euler method. In [24], a novel discrete-time field-oriented model was derived from a stationary model obtained with a variational integrator, for instance, the SEM [25] (The SEM yields DTMs that better represent the sampled dynamics of continuous-time systems at lower sampling rates). Then, a discrete-time controller was proposed. Despite the novelties presented in this article, the discrete-time field-oriented model does not resemble the dc motor with separated excitation; hence, the decoupling between the rotor velocity and the rotor flux modulus control designs was not properly achieved.

The aims of this article are the following: 1) to obtain a novel DTM oriented to the field for IMs with decoupled rotor velocity and rotor flux modulus dynamics; 2) to establish the basics of FOC design in discrete time for direct and indirect versions; and 3) the comparison of their performances with respect to discretized versions of FOCs, to establish which ensures better results with different sampling periods. In order to achieve decoupling of the rotor velocity and the rotor flux modulus, the DTM presented in [24] is further enhanced. Then, based on the decoupled DTM, procedures for designing discrete-time controllers oriented to the field in direct and indirect versions are provided.

The novel contributions of this article are as follows.

A novel DTM oriented to the field for IMs is presented. The advantages of this model are as follows.

1) It comes from a DTM in the stationary reference frame [25] that better approximates the sampled dynamics with relatively low sampling rates for IMs by using a variational integrator.
2) The proposed model is consistent with the continuous-time counterpart, i.e., it is linear, and the rotor velocity and rotor flux dynamics are decoupled, which will allow us to design controllers more straightforwardly in a discrete-time setting.
3) Designed controllers based on the proposed model will take full advantage of digital signals (sampled currents and digital rotor velocity from an encoder), as the signals provided by the proposed model match with the digital signals.
4) Designed controllers can be directly implemented in any digital device without approximations.

Novel discrete-time controllers oriented to the field in direct and indirect versions for IMs are designed. The advantages of these controllers are as follows.

1) In the case of classical proportional–integral (PI) controllers, the stability analysis of the closed-loop linear system is carried out with the easiness of the eigenvalues placement.
2) The proposal of reference signals for stator currents and stator voltages is more straightforward.
3) The proposed controllers can perform better at lower sampling rates than the approximated continuous-time counterparts. This fact is very attractive, since high-end digital devices are not required, resulting in a low-cost implementation.
4) Researchers can enhance the proposed controllers by replacing PI control loops with robust or modern controllers, as done in existing works in the continuous-time domain, and, in this way, by taking advantage of the previously mentioned advantages.

The rest of this article is organized as follows. In Section II, decoupling of the DTM of the IM oriented to the field is presented. In Section III, discrete-time direct and indirect FOCs are designed. Simulation and experimental results are presented in Sections IV and V, respectively. Finally, Section VI concludes this article.

II. Discrete-Time Field-Oriented Model

Based on [24], the discrete-time IM model in a generic rotating (d, q) reference frame is presented in scalar form as follows:

$$\begin{aligned}
\omega_{k+1} &= \omega_k + \frac{T_s}{J}\tau_{e,k} - \frac{T_s}{J}\tau_{L,k} \\
\phi_{d,k+1} &= \frac{1}{\tau_{rd}}\varphi_1(\omega_{s,k}, \phi_{d,k}, \phi_{q,k}) + \frac{T_s L_m}{\tau_r \tau_{rd}}\varphi_1(\omega_{s,k}, i_{d,k}, i_{q,k}) \\
\phi_{q,k+1} &= \frac{1}{\tau_{rd}}\varphi_2(\omega_{s,k}, \phi_{d,k}, \phi_{q,k}) + \frac{T_s L_m}{\tau_r \tau_{rd}}\varphi_2(\omega_{s,k}, i_{d,k}, i_{q,k}) \\
i_{d,k+1} &= \gamma_d \varphi_1(\omega_{\phi,k}, i_{d,k}, i_{q,k}) + \frac{\beta_d}{\tau_{rd}}\varphi_1(\omega_{\phi,k}, \phi_{d,k}, \phi_{q,k}) \\
&\quad - \frac{\beta_d}{\tau_{rd}^2}\varphi_1(\omega_{s,k}, \psi_{d,k}, \psi_{q,k}) + \frac{T_s}{\sigma_d}\varphi_1(\omega_{\phi,k}, u_{d,k}, u_{q,k}) \\
i_{q,k+1} &= \gamma_d \varphi_2(\omega_{\phi,k}, i_{d,k}, i_{q,k}) + \frac{\beta_d}{\tau_{rd}}\varphi_2(\omega_{\phi,k}, \phi_{d,k}, \phi_{q,k}) \\
&\quad - \frac{\beta_d}{\tau_{rd}^2}\varphi_2(\omega_{s,k}, \psi_{d,k}, \psi_{q,k}) + \frac{T_s}{\sigma_d}\varphi_2(\omega_{\phi,k}, u_{d,k}, u_{q,k})
\end{aligned} \tag{1}$$

with

$$\tau_{e,k} = \frac{k_T}{\tau_{r,d}}\phi_{d,k} i_{q,k} \tag{2}$$

$$\omega_{s,k} = \omega_{\phi,k} - p\omega_k. \tag{3}$$

Field orientation of model (1) is achieved when $\phi_{q,k} = 0\,\forall k$, i.e., the d-axis of the rotating reference frame is aligned with the

rotor flux vector. Now, by using this condition, we obtain the following relation from the difference equation of $\phi_{q,k+1}$ in (1):

$$i_{q,k} = \frac{\tau_r \sin T_s\omega_{s,k}}{L_m T_s \cos T_s\omega_{s,k}}\phi_{d,k} + \frac{\sin T_s\omega_{s,k}}{\cos T_s\omega_{s,k}} i_{d,k}. \tag{4}$$

Now, relations $\phi_{q,k} = 0$ and (4) are substituted into the electrical variables of (1), yielding the following discrete-time field-oriented model:

$$\begin{aligned}
\omega_{k+1} &= \omega_k + \frac{T_s}{J}\tau_{e,k} - \frac{T_s}{J}\tau_{L,k} \\
i_{q,k+1} &= f_{q,k} + \frac{T_s}{\sigma_d}\left(-\sin(T_s\omega_{\phi,k})u_{d,k} + \cos(T_s\omega_{\phi,k})u_{q,k}\right) \\
\phi_{d,k+1} &= \frac{1}{\tau_{rd}}\frac{1}{\cos(T_s\omega_{s,k})}\phi_{d,k} + \frac{T_s L_m}{\tau_r \tau_{rd}}\frac{1}{\cos(T_s\omega_{s,k})} i_{d,k} \\
i_{d,k+1} &= f_{d,k} + \frac{T_s}{\sigma_d}\left(\cos(T_s\omega_{\phi,k})u_{d,k} + \sin(T_s\omega_{\phi,k})u_{q,k}\right)
\end{aligned} \tag{5}$$

where

$$\begin{aligned}
f_{d,k} &= \gamma_d \frac{\cos(T_s p\omega_k)}{\cos(T_s\omega_{s,k})} i_{d,k} - \frac{\beta_d T_s L_m}{\tau_{rd}^2 \tau_r}\frac{1}{\cos(T_s\omega_{s,k})} i_{d,k} \\
&\quad + \frac{\gamma_d \tau_r}{T_s L_m}\frac{\sin(T_s\omega_{\phi,k})\sin(T_s\omega_{s,k})}{\cos(T_s\omega_{s,k})}\phi_{d,k} \\
&\quad + \frac{\beta_d}{\tau_{rd}}\cos(T_s\omega_{\phi,k})\phi_{d,k} - \frac{\beta_d}{\tau_{rd}^2}\frac{1}{\cos(T_s\omega_{s,k})}\phi_{d,k} \\
f_{q,k} &= -\gamma_d \sin(T_s p\omega_k) i_{d,k} - \frac{2\beta_d T_s L_m}{\tau_{rd}^2 \tau_r}\sin(T_s\omega_{s,k}) i_{d,k} \\
&\quad + \frac{\gamma_d \tau_r}{T_s L_m}\frac{\cos(T_s\omega_{\phi,k})\sin(T_s\omega_{s,k})}{\cos(T_s\omega_{s,k})}\phi_{d,k} \\
&\quad - \frac{\beta_d}{\tau_{rd}}\sin(T_s\omega_{\phi,k})\phi_{d,k}.
\end{aligned} \tag{6}$$

The current dynamics in (5) are linearized with the following feedback that cancels out the old dynamics (6) and introduces the new dynamics with pole location at γ_d and the virtual controls $v_{d,k}$ and $v_{q,k}$:

$$\begin{aligned}
u_{d,k} &= \frac{\sigma_d}{T_s}\cos(T_s\omega_{\phi,k})\left(\gamma_d i_{d,k} - f_{d,k} + v_{d,k}\right) \\
&\quad - \frac{\sigma_d}{T_s}\sin(T_s\omega_{\phi,k})\left(\gamma_d i_{q,k} - f_{q,k} + v_{q,k}\right) \\
u_{q,k} &= \frac{\sigma_d}{T_s}\sin(T_s\omega_{\phi,k})\left(\gamma_d i_{d,k} - f_{d,k} + v_{d,k}\right) \\
&\quad + \frac{\sigma_d}{T_s}\cos(T_s\omega_{\phi,k})\left(\gamma_d i_{q,k} - f_{q,k} + v_{q,k}\right).
\end{aligned} \tag{7}$$

Feedback (7) yields a decoupled discrete-time field-oriented model as

$$\Sigma_\omega : \begin{cases} \omega_{k+1} = \omega_k + \frac{T_s}{J}\tau_{e,k} - \frac{T_s}{J}\tau_{L,k} \\ i_{q,k+1} = \gamma_d i_{q,k} + v_{q,k} \end{cases} \tag{8}$$

$$\Sigma_\phi : \begin{cases} \phi_{d,k+1} = \eta_{2,k}\phi_{d,k} + \eta_{3,k} i_{d,k} \\ i_{d,k+1} = \gamma_d i_{d,k} + v_{d,k} \end{cases} \tag{9}$$

It is worth mentioning that the proposed model (8), (9) is composed of two subsystems: the rotor velocity subsystem Σ_ω, and the rotor flux subsystem Σ_ϕ. Subsystem Σ_ϕ is linear and uncoupled. Once $\phi_{d,k}$ has reached a constant steady state, subsystem Σ_ω is assumed to be linear and uncoupled too, where linear control methods can be directly applied. In contrast, the model presented in [25] is coupled and nonlinear, and the model presented in [24] is actually in a generic rotating (d, q) reference frame, where the IM is still presented as a coupled and nonlinear system.

III. DTFOC

Considering an IM fed by a voltage-controlled inverter, the control problem is to design voltage signals that can regulate ω_k and $\phi_{d,k}$ for tracking of some desired reference signals $\omega_{r,k}$ and $\phi_{d,r,k}$, ensuring at the same time the rejection of an unknown constant load torque.

Under a field orientation context, when measurements of the rotor flux vector are available, direct field orientation can be achieved. Direct field orientation can also be achieved at least with the estimation of such a vector. If no measurements or estimations of the rotor flux vector are available, then the angle of the rotor flux vector is calculated with an integral operation, yielding indirect field orientation.

A. DTDFOC Design

In order to solve the posed control problem, virtual controls are proposed as current (inner) control loops that cancel out the old current error dynamics and introduce the new one as PI actions

$$\begin{aligned}
v_{d,k} &= k_{21}(i_{d,k} - i_{d,r,k}) + k_{22}\sum_{n=1}^{k} T_s(i_{d,n-1} - i_{d,r,n-1}) \\
&\quad - a_1 i_{d,k} + a_2\phi_{d,k} + \frac{k_{12}}{\eta_3}\sum_{n=1}^{k} T_s\chi_{d,n-1}
\end{aligned} \tag{10}$$

$$\begin{aligned}
v_{q,k} &= k_{41}(i_{q,k} - i_{q,r,k}) + k_{42}\sum_{n=1}^{k} T_s(i_{q,n-1} - i_{q,r,n-1}) \\
&\quad - a_4 i_{q,k} + a_5\omega_k + \frac{k_{32}}{a_3}\sum_{n=1}^{k} T_s\chi_{q,n-1}.
\end{aligned} \tag{11}$$

Reference signals for stator currents are proposed as rotor flux and rotor velocity (outer) control loops that cancel out old output error dynamics and introduce the new one as PI actions:

$$\begin{aligned}
i_{d,r,k} &= \frac{k_{11}}{\eta_3}(\phi_{d,k} - \phi_{d,r,k}) + \frac{k_{12}}{\eta_3}\sum_{n=1}^{k} T_s(\phi_{d,n-1} - \phi_{d,r,n-1}) \\
&\quad - \frac{\eta_2}{\eta_3}\phi_{d,k}
\end{aligned} \tag{12}$$

$$\begin{aligned}
i_{q,r,k} &= \frac{k_{31}}{a_3}(\omega_k - \omega_{r,k}) + \frac{k_{32}}{a_3}\sum_{n=1}^{k} T_s(\omega_{n-1} - \omega_{r,n-1}) \\
&\quad - \frac{1}{a_3}\omega_k.
\end{aligned} \tag{13}$$

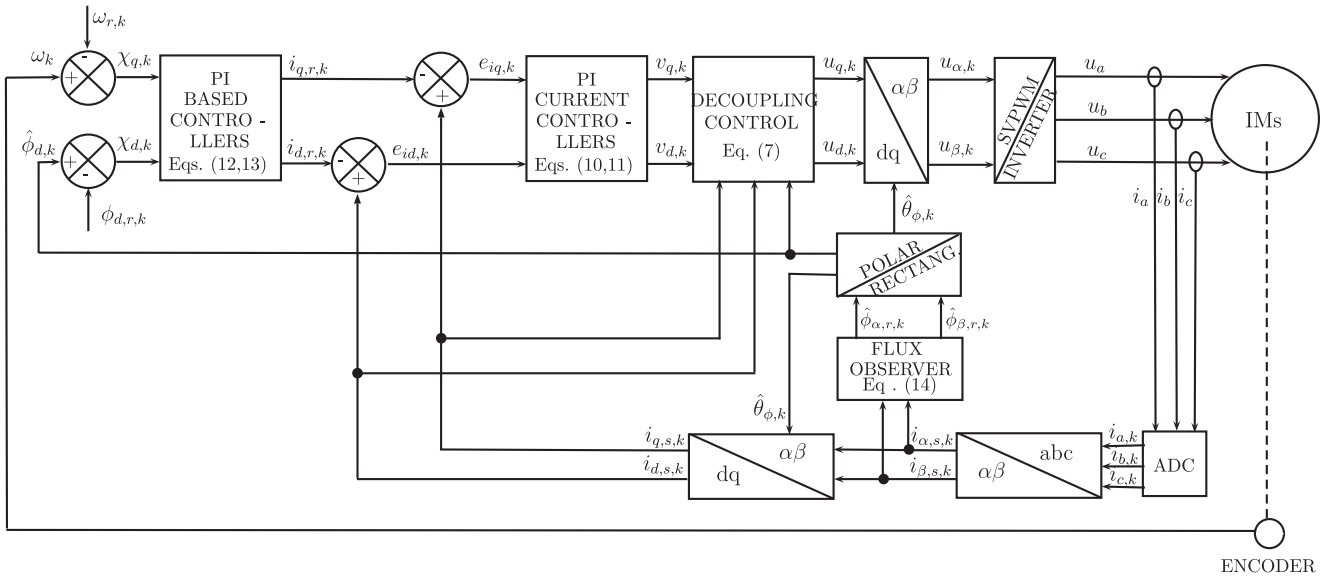

Fig. 1. Block diagram of the proposed discrete-time direct field-oriented controller.

See Appendix A1 for the closed-loop stability analysis of (9)–(11).

On the other hand, rotor flux measurement is commonly not carried out due to the lack of space for arranging sensors inside the motor, or the sensors are expensive; however, rotor flux estimation is a common task. For that, the proposed rotor flux observer in [26], in the stationary reference frame (α, β), is here used and presented as

$$\hat{\Phi}_{r,k+1} = \frac{1}{\tau_{r,d}} e^{\mathcal{J} T_s p w_k} \hat{\Phi}_{r,k} + T_s \frac{L_m}{\tau_r \tau_{r,d}} e^{\mathcal{J} T_s p w_k} I_{s,k}. \quad (14)$$

The angle of the rotor flux in the stationary reference frame and the rotor flux vector are determined as

$$\hat{\theta}_{\phi,k} = \arctan(\hat{\phi}_{\beta,r,k} / \hat{\phi}_{\alpha,r,k}) \quad (15)$$

$$\hat{\Phi}_{d,q,k} = e^{-\mathcal{J} \hat{\theta}_{\phi,k}} \hat{\Phi}_{r,k} \quad (16)$$

with $\mathcal{J}$ being a skew-symmetric matrix. Finally, Fig. 1 shows a block diagram of the proposed control scheme.

B. DTIFOC Design

Given $\phi_{d,r,k}$ as a desired reference constant signal for the rotor flux, the corresponding reference signal for $i_{d,k}$, i.e., $i_{d,r,k}$, can be determined from the first equation in (9) as

$$i_{d,r,k} = \frac{1 - \eta_2}{\eta_3} \phi_{d,r,k}. \quad (17)$$

The stator voltage $v_{d,k}$ is proposed as a PI action

$$v_{d,k} = \kappa_{11}(i_{d,k} - i_{d,r,k}) + \kappa_{12} \sum_{n=1}^{k} T_s (i_{d,n-1} - i_{d,r,n-1}). \quad (18)$$

Control action (18) guarantees that the tracking error for $i_{d,k}$ is equal to zero; this means that the desired current $i_{d,r,k}$ is circulating in the IM and imposes the desired rotor flux $\phi_{d,r,k}$.

On the other hand, given a reference signal $\omega_{r,k}$ for the rotor velocity, the reference signal for the electromagnetic torque is proposed as a PI action

$$\tau_{e,r,k} = \frac{J}{T_s} \left(\kappa_{21}(\omega_k - \omega_{r,k}) + \kappa_{22} \sum_{n=1}^{k} T_s (\omega_{n-1} - \omega_{r,n-1}) \right). \quad (19)$$

Then, the desired q component of the stator current, i.e., $i_{q,r,k}$, can be determined from the desired version of (2) as

$$i_{q,r,k} = \frac{\tau_{r,d} \tau_{e,r,k}}{k_T \phi_{d,r,k}}. \quad (20)$$

The stator voltage $v_{q,k}$ is then proposed as a PI action

$$v_{q,k} = \kappa_{31}(i_{q,k} - i_{q,r,k}) + \kappa_{32} \sum_{n=1}^{k} T_s (i_{q,n-1} - i_{q,r,n-1}). \quad (21)$$

See Appendix A2 for the closed-loop stability analysis of (9), (18), and (21).

For determining the angle of the rotor flux vector, let us consider the integration of the angular velocity of the rotor flux vector in (3) as

$$\theta_{\phi,k} = \sum_{n=1}^{k} T_s \omega_{\phi,n-1}. \quad (22)$$

Taking one step ahead of (22), we obtain

$$\theta_{\phi,k+1} = \theta_{\phi,k} + T_s \omega_{\phi,k} = \theta_{\phi,k} + T_s p \omega_k + T_s \omega_{s,k} \quad (23)$$

where the slip angular velocity in (23) is calculated from (4) as a required signal for field orientation achievement

$$\omega_{s,r,k} = \frac{1}{T_s} \arctan \left(\frac{L_m T_s i_{q,r,k}}{\tau_r \phi_{d,r,k} + L_m T_s i_{d,r,k}} \right) \quad (24)$$

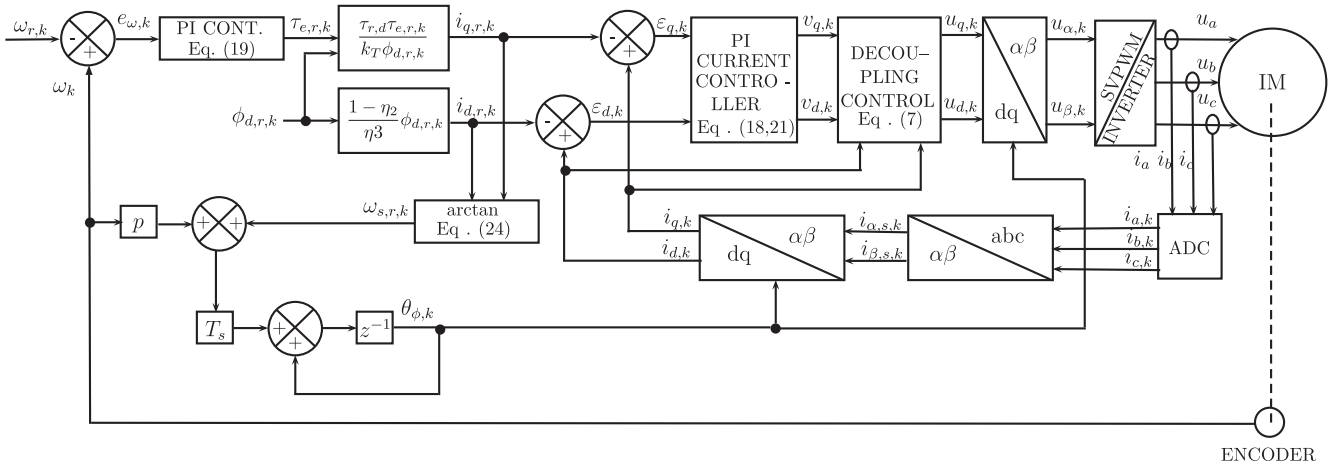

Fig. 2. Block diagram of the proposed discrete-time indirect field-oriented controller.

with $i_{d,r,k}$ and $i_{q,r,k}$ already defined in (17) and (20), respectively. Finally, Fig. 2 shows a block diagram of the proposed control scheme.

Remark 3.1: Although the proposed DTFOC-based PI controllers represent the most basic designs, standard FOC principles have been properly extended to the discrete-time setting. The PI actions can be replaced with novel discrete-time control techniques, which will permit researchers to take full advantage of the acquired digital signals provided by the analog-to-digital converter and the encoder (both shown in Figs. 1 and 2).

C. Comparison With Similar Works

In [26], two controllers based on sliding-mode techniques are presented: Type I is based on the equivalent control method for the inner control loop and on a proportional controller for the outer control loop. The equivalent control method cancels out all linear and nonlinear terms behaving like a dead-beat-type controller, where the demand of control resources is high, requiring a saturation stage. The stability analysis during the linear section of the saturation stage is trivial, but not during saturation, where more specialized analysis is required. The type II controller is based on the supertwisting algorithm (STA) for the inner control loop and on a PI controller for the outer control loop. The main disadvantage of the type I controller is that it requires knowledge of parameters and perturbations. This disadvantage is overcome with the type II controller as the STA does require knowledge for only the upper bound of perturbations, but the stability analysis of the closed-loop nonlinear system is carried out with the proposal of a Lyapunov function.

On the other hand, in [24], the inner and outer control loops are based on PI controllers. It is well known that integral actions can only cancel out constant perturbations, and due to the presentation of the model as a coupled and nonlinear system, the general control design is based on the nonlinear block control technique [27], where the system is linearized, and the stability analysis is carried out with linear methods.

Finally, in our proposal, the inner and outer control loops are also based on PI controllers, where the control design is easier to carry out, i.e., the proposal of reference signals for the stator currents and the stator voltages is more straightforward than those presented in [24] and [26], in a similar fashion to those in the continuous-time setting, where the stability analysis of the closed-loop linear system can be carried out with the easiness of the eigenvalue placement.

TABLE I
PARAMETER VALUES OF THE PROPOSED DTM FOR ALL THREE SAMPLING PERIODS USED IN SIMULATIONS

$T_s\,(\mu\text{s})$	$1/\tau_{r,d}$	$\sigma_d(\text{H})$	γ_d	$\beta_d\,(1/\text{H})$	$\mu_d(1/\text{kgm}^2)$
100	0.9995	0.0119	0.9907	81.420	145.632
600	0.9969	0.0124	0.9462	78.088	145.258
3000	0.9847	0.0148	0.7747	65.425	143.485

IV. SIMULATIONS

The proposed control algorithms are numerically simulated. For that, we have considered an IM with the following nameplate data: three phases, 3 hp, 1750 r/min, 220 V, and 60 Hz. The constant parameters that depend on the sampling period are shown in Table I.

The performance of the proposed controllers that are based on the novel discrete-time field-oriented model (9) is studied in simulations for three different sampling periods (100, 600, and 3000 μs). For comparison purposes, SDFOC and SIFOC controllers (see Appendix B) by means of the explicit Euler method are also simulated. The load torque is fixed at the constant value of 5.5 N· m, but during the time interval 4.5–5.5 s, the load torque is incremented up to 11 N· m. The load torque is considered unknown for the controllers. All the PI gains were initially designed as in Appendix A1 and then fine-tuned for better results. Proposed gains are shown in Table II.

The reference signal for the rotor flux modulus is 0.25 Wb, but during the time interval 2.5–3.5 s, it is incremented up to 0.4 Wb. The rotor velocity reference signal is initiated with a ramp, followed of a series of steps, as illustrated in the following figures. The introduced steps in the reference signals are for verifying the

TABLE II
CONTROLLER GAINS

T_s	DTDFOC	SDFOC	DTIFOC	SIFOC
100μs	k_{11}=0.9752	p_{d1}=248	κ_{11}=−0.9	c_1=250
	k_{12}=−1.5376	p_{d2}=15376	κ_{12}=−0.0005	c_2=5
	k_{21}=0.9875	p_{q1}=248	κ_{21}=−0.055	c_{d1}=9800
	k_{22}=−0.3881	p_{q2}=15376	κ_{22}=−0.00034	c_{d2}=350
	k_{31}=0.9752	$\bar{p}_{d1}$=2050	κ_{31}=−1.6	c_{q1}=9800
	k_{32}=−1.5378	$\bar{p}_{d2}$=2000	κ_{32}=−0.0005	c_{q2}=350
	k_{41}=0.9875	$\bar{p}_{q1}$=2050		
	k_{42}=−0.3881	$\bar{p}_{q2}$=2000		
600μs	k_{11}=0.8554	p_{d1}=240	κ_{11}=−0.9	c_1=450
	k_{12}=−8.7016	p_{d2}=14502	κ_{12}=−0.005	c_2=15
	k_{21}=0.9160	p_{q1}=240	κ_{21}=−0.3	c_{d1}=500
	k_{22}=−2.9332	p_{q2}=14502	κ_{22}=−0.05	c_{d2}=1550
	k_{31}=0.8554	$\bar{p}_{d1}$=1139	κ_{31}=−1.5	c_{q1}=678
	k_{32}=−8.7016	$\bar{p}_{d2}$=1888	κ_{32}=−0.005	c_{q2}=3550
	k_{41}=0.9160	$\bar{p}_{q1}$=1139		
	k_{42}=−2.9332	$\bar{p}_{q2}$=1888		
3000μs	k_{11}=0.6580	p_{d1}=227	κ_{11}=−0.998	c_1=280
	k_{12}=−19.487	p_{d2}=12991	κ_{12}=−0.0005	c_2=16
	k_{21}=0.7967	p_{q1}=227	κ_{21}=−1.41	c_{d1}=274
	k_{22}=−6.8820	p_{q2}=12991	κ_{22}=−0.062	c_{d2}=10
	k_{31}=0.6580	$\bar{p}_{d1}$=181	κ_{31}=−1.43	c_{q1}=678
	k_{32}=−19.487	$\bar{p}_{d2}$=7720	κ_{32}=−0.041	c_{q2}=3550
	k_{41}=0.7967	$\bar{p}_{q1}$=181		
	k_{42}=−6.8820	$\bar{p}_{q2}$=7720		

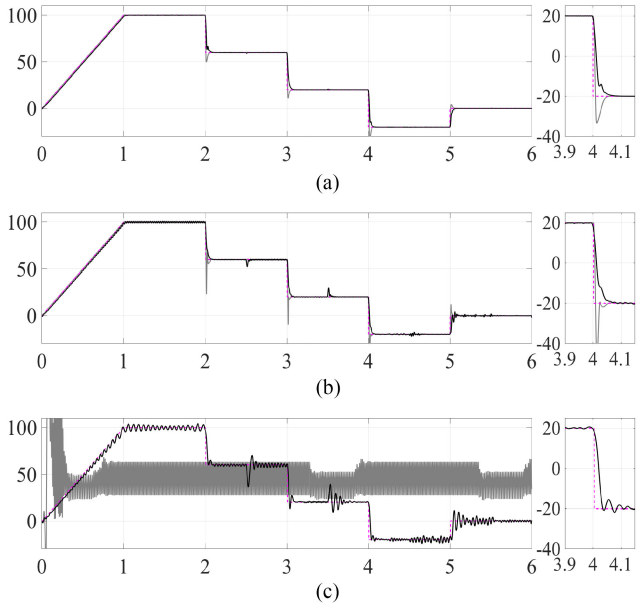

Fig. 3. Simulated rotor velocity profiles with controllers implemented with sampling times [rad/s versus s]: (a) $T_s = 100$ μs, (b) $T_s = 600$ μs, and (c) $T_s = 3000$ μs. Reference signal (magenta-dashed), proposed DTDFOC (black-solid), and SDFOC (gray-solid).

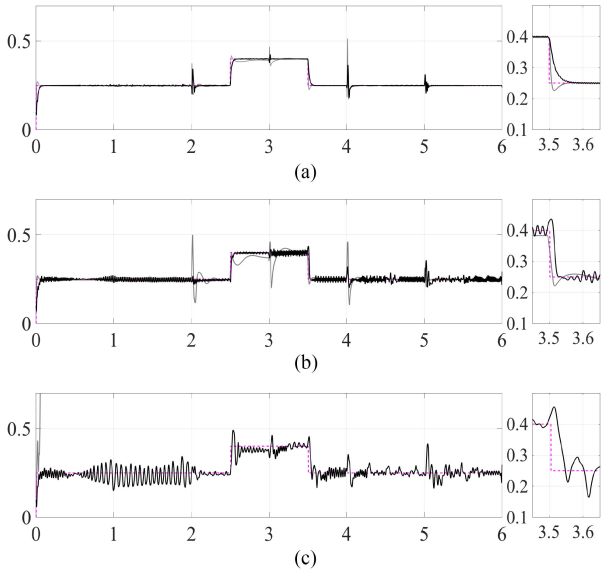

Fig. 4. Simulated rotor flux modulus profiles with controllers implemented with sampling times [Wb versus s]: (a) $T_s = 100$ μs, (b) $T_s = 600$ μs, and (c) $T_s = 3000$ μs. Reference signal (magenta-dashed), proposed DTDFOC (black–solid), and SDFOC (gray-solid).

tracking performance of the controllers. The computation delay and the zero-order-hold behavior of pulsewidth modulation are considered by inserting two sampling period delays (see [29] for details).

Simulation results for output tracking of the proposed DTDFOC and the SDFOC are shown in Figs. 3, and 4. The performance of the rotor velocity for the DTDFOC is good; just small oscillations are appreciated with a sampling period of $T_s = 3000$ μs. Similar arguments can be noted for the SFOC, but for $T_s = 3000$ μs, the closed-loop IM cannot be stabilized. With respect to the rotor flux modulus, in the case of the DTDFOC, with a sampling period of $T_s = 100$ μs, the accuracy is good, with $T_s = 600$ μs, the tracking accuracy is good but with noise, and with $T_s = 3000$ μs, the noise is incremented. In the case of the SFOC, a good tracking accuracy is noted with $T_s = 100$ μs; with $T_s = 600$ μs, some tracking mismatches are observed, but with $T_s = 3000$ μs, tracking capabilities are lost. This can be attributable to the fact that the discrete-time approximation of the observer for rotor fluxes (46) deteriorates as the sampling period increases. Using large sampling periods makes the accuracy of the control equations to be lost (due to discretetized model mismatches); hence, output tracking errors start to increase, and the controllers start to produce large control actions. Control actions will rapidly reach the maximum control resources and will act as saturated controllers that can make the control actions to rapidly excurse from the upper to the lower saturation value, and vice versa, for all subsequent time. This issue makes the IM outputs deviate from the reference signals. This problem resembles to the chattering phenomenon (small oscillations at the outputs) that occurs with sliding-mode controllers [30].

In the case of indirect controllers, simulations are shown in Figs. 5 and 6. With respect to direct controllers, indirect controllers yield smoother responses, which can be attributable to the absence of the rotor flux observer dynamics, which tend to deteriorate as the sampling period increases. It can be noted that the proposed DTIFOC yields similar responses to that obtained with the SIFOC; just small differences are observed in rotor flux modulus tracking with a sampling period of 600 μs, where the proposed DTIFOC is slightly more accurate than the SIFOC. With a sampling period of 3000 μs, in the SIFOC, the rotor velocity is characterized by noise, and the rotor flux modulus tracking

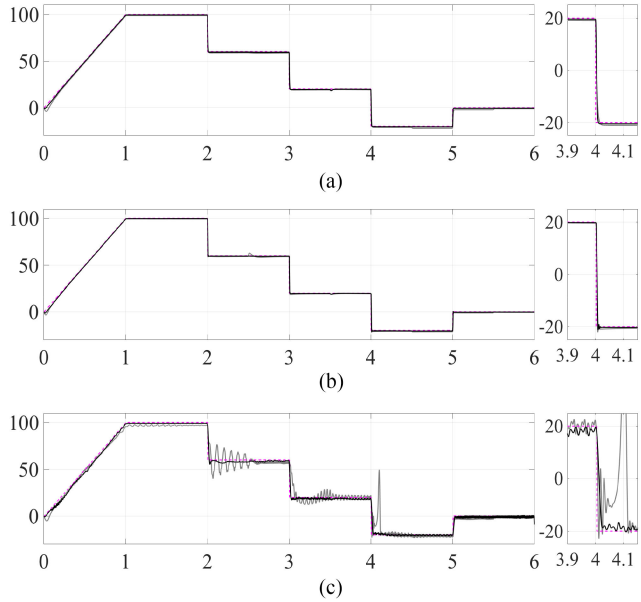

Fig. 5. Simulated rotor velocity profiles with controllers implemented with sampling times[rad/s versus s]: (a) $T_s = 100$ μs, (b) $T_s = 600$ μs, and (c) $T_s = 3000$ μs. Reference signal (magenta-dashed), proposed DTIFOC (black-solid), and SIFOC (gray-solid).

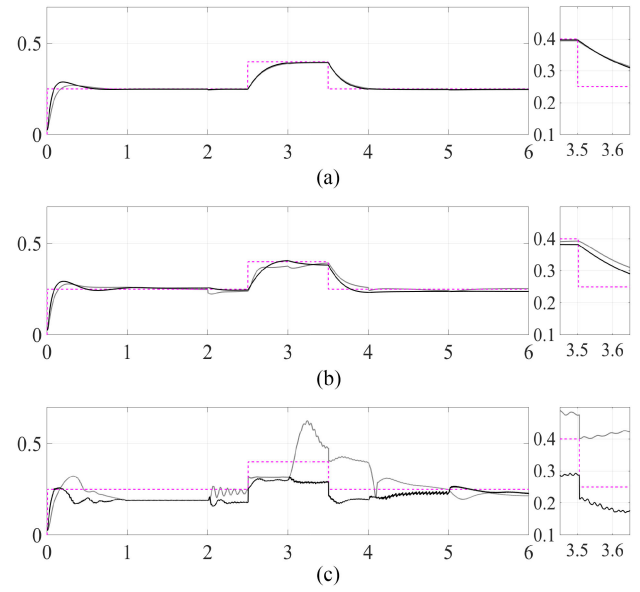

Fig. 6. Simulated rotor flux modulus profiles with controllers implemented with sampling times [Wb versus s]: (a) $T_s = 100$ μs, (b) $T_s = 600$ μs, and (c) $T_s = 3000$ μs. Reference signal (magenta-dashed), proposed DTIFOC (black-solid), and SIFOC (gray-solid).

performance is poor; this fact can be attributable to discrete-time approximations of the integral actions of the PI control loops. The SDFOC and the SIFOC are negatively affected with large sampling periods due to the fact that the sampled dynamics of the IM were not taken into account.

In general, for both direct and indirect controllers, it can be observed that the load torque pulse introduced at time 4.5 s does slightly affect the mechanical dynamics, but not the rotor flux dynamics, due to the decoupling control (7). Fig. 7 shows the

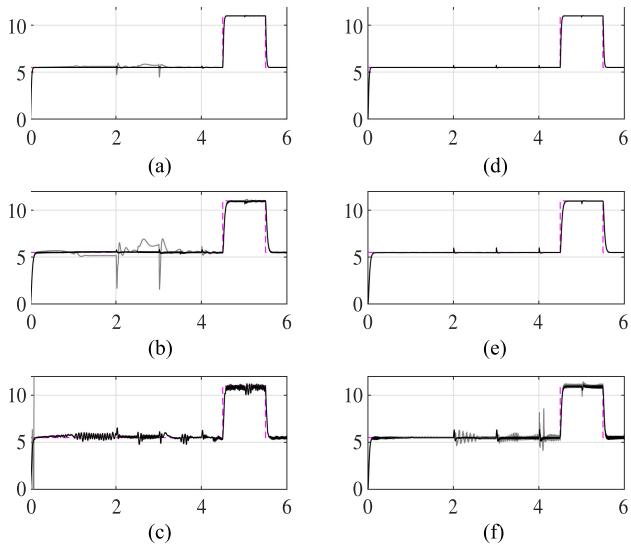

Fig. 7. Simulated load torque estimations [N·m versus s]. Direct FOCs: (a) $T_s = 100$ μs, (b) $T_s = 600$ μs, and (c) $T_s = 3000$ μs. Indirect FOCs: (d) $T_s = 100$ μs, (e) $T_s = 600$ μs, and (f) $T_s = 3000$ μs. Applied load torque (magenta-dashed), proposed controller (black-solid), and sampled controller (gray-solid).

TABLE III
PRECISION ERROR AND SETTLING TIME EVALUATION FOR TRACKING OF THE ROTOR VELOCITY IN SIMULATIONS

	100 μs		600 μs		3000 μs	
	$P_e(\%)$	t_s(s)	$P_e(\%)$	t_s(s)	$P_e(\%)$	t_s(s)
DTDFOC	0.005	0.05	0.03	0.05	0.135	0.1
SDFOC	0.0	0.05	0.0	0.05	–	–
DTIFOC	0.9	0.01	2.0	0.012	2.9	0.025
SIFOC	5.5	0.015	5.7	0.012	10.8	0.12

TABLE IV
PRECISION ERROR AND SETTLING TIME EVALUATION FOR TRACKING OF THE ROTOR FLUX MODULUS IN SIMULATIONS

	100 μs		600 μs		3000 μs	
	$P_e(\%)$	t_s(s)	$P_e(\%)$	t_s(s)	$P_e(\%)$	t_s(s)
DTDFOC	0.0625	0.05	1.375	0.05	0.5875	0.13
SDFOC	1.9	0.05	7.1	0.01	–	–
DTIFOC	0.875	0.5	4.45	0.5	29.5	–
SIFOC	1.675	0.5	6.0	0.5	51.175	–

simulation results for load torque estimations for the proposed controllers and the corresponding sampled versions. Such estimations are provided by the integral actions in outer control loops (see Appendix A1).

Simulation results are summarized in Tables III and IV, where the precision error $P_e = 100|S_r - Av_{ss}|/S_r$ (the absolute difference between the average steady-state output signal Av_{ss}, and its reference value S_r, divided by the reference value), and the settling time values are presented. It is worth mentioning that P_e is calculated in a constant section of a graph with the worst tracking performance, and in the case of an output signal to be symmetrically oscillating around the reference signal, the precision error will be zero regardless of the amplitude of the oscillations.

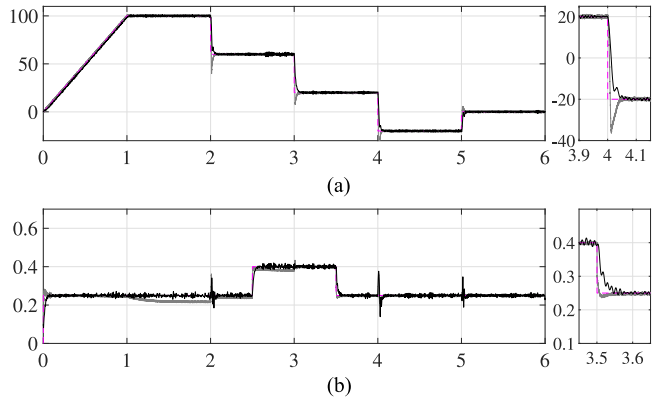

Fig. 8. Real-time output profiles implemented with a sampling time of $T_s = 100\ \mu$s. (a) Rotor velocity tracking [rad/s versus s]. (b) Rotor flux modulus tracking [Wb versus s]. Reference signal (magenta-dashed), proposed DTDFOC (black-solid), and SDFOC (gray-solid).

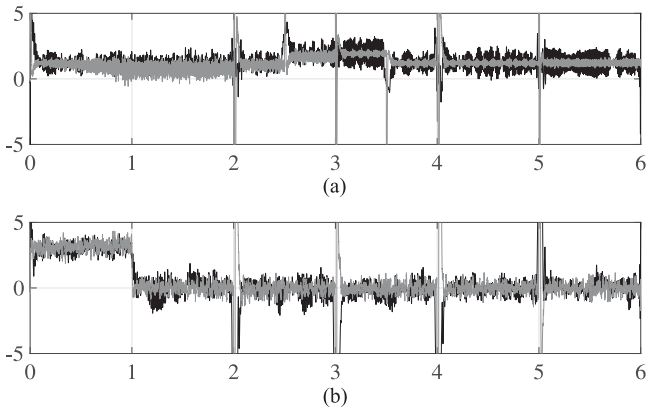

Fig. 9. Real-time stator currents components for a sampling time of $T_s = 100\ \mu$s. (a) $i_{d,k}$ [A versus s]. (b) $i_{q,k}$ [A versus s]. Proposed DTDFOC (black-solid) and SDFOC (gray-solid).

V. Real-Time Experiments

The IM under test has the same parameter values of the simulated motor in Section IV. The experimental setup consists of a three-phase voltage source supplied to a three-phase variable transformer (VARIAC). These voltages are fed into a power module (Semikron IGBT Power Electronics Teaching System), which incorporates a three-phase rectifier and an inverter. The control algorithm is programmed in Simulink and implemented with a DSP board (DSpace 1104). The board's library is used to decode the position from the encoder digital signals. The velocity is then calculated by taking the position change rate and by filtering it with a first-order Butterworth low-pass filter with 8-rad/s edge frequency, in order to attenuate the measurement noise. The stator phase currents are measured by Hall-type sensors (LEM HX 10-P). The IM is loaded with a flywheel that supplies a load torque proportional to the time derivative of the rotor velocity, which is considered unknown. Reference signals for the rotor velocity and the rotor flux modulus are the same as those used in simulations.

The obtained results for a sampling period of 100 μs are shown in Fig. 8, where the measured rotor velocity and the estimated rotor flux modulus are presented. Both controllers, i.e., DTDFOC and SDFOC, perform tracking of the rotor velocity reference signal with good accuracy. For tracking the rotor flux modulus reference signal, the DTDFOC performs better than the SDFOC in terms of accuracy that can be attributable to the fact that DTDFOC takes into account the sampled dynamics of IMs.

The profiles for stator currents in the (d, q) reference frame are shown in Fig. 9. It can be appreciated that $i_{d,k}$ profiles are consistent with the rotor flux modulus, i.e., there are increments at the time interval (2.5–3.5 s), just as shown by the rotor flux modulus. As already mentioned, the load torque is proportional to the time derivative of the rotor velocity; this means that the load torque is constant in the time interval (0–1 s) and zero for the rest of the time, except at the step increments or decrements, where the load torque is characterized by peaks. Hence, $i_{q,k}$ profiles are consistent with the load torque.

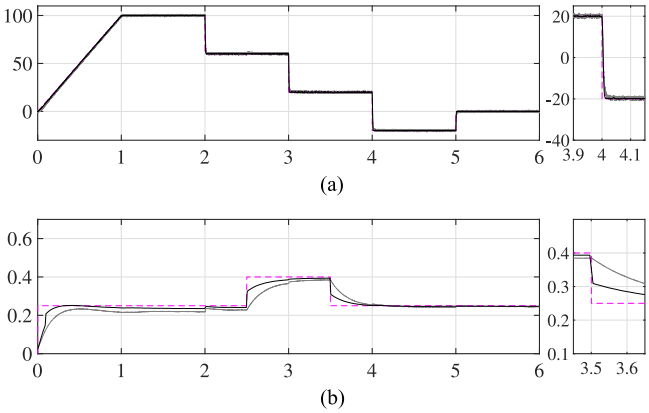

Fig. 10. Real-time output profiles implemented with a sampling time of $T_s = 100\ \mu$s. (a) Rotor velocity tracking [rad/s versus s]. (b) Rotor flux modulus tracking [Wb versus s]. Reference signal (magenta-dashed), proposed DTIFOC (black-solid), and SIFOC (gray-solid).

Corresponding results for indirect controllers, DTIFOC and SIFOC, with a sampling period of 100 μs are shown in Figs. 10 and 11 for outputs and currents, respectively. Note good accuracy provided by indirect controllers and a smoother response than that of direct controllers that can be attributable to the absence of a rotor flux observer. But the proposed DTIFOC performs better than the SIFOC.

Fig. 12 shows the corresponding outputs for direct controllers with a sampling time of $T_s = 600\ \mu$s, where the measured rotor velocity and the estimated rotor flux modulus are presented. Good performance for tracking of the rotor velocity for both controllers can still be observed. The rotor flux modulus in the case of DTDFOC suffers from noise, and in the case of SDFOC, it suffers from a loss in accuracy, as predicted by simulations. Fig. 13 shows the current profiles. These are noisy signals, where consistencies observed for the case of $T_s = 100\ \mu$s are mildly detected.

The corresponding results for indirect controllers are shown in Figs. 14 and 15. It can be noted that both controllers, i.e., DTIFOC and SIFOC, still perform with good accuracy, and that current profiles are still consistent as mentioned by previous

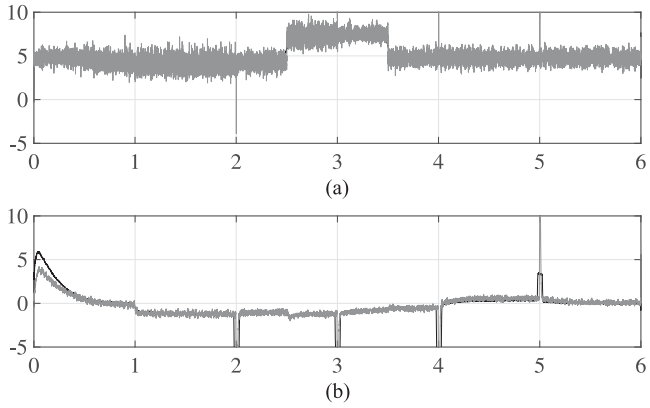

Fig. 11. Real-time stator currents components for a sampling time of $T_s = 100\ \mu$s. (a) $i_{d,k}$ [A versus s]. (b) $i_{q,k}$ [A versus s]. Proposed DTIFOC (black-solid) and SIFOC (gray-solid).

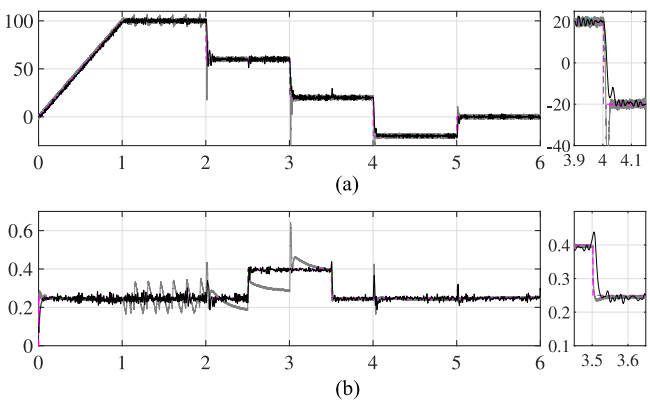

Fig. 12. Real-time output profiles implemented with a sampling time of $T_s = 600\ \mu$s. (a) Rotor velocity tracking [rad/s versus s]. (b) Rotor flux modulus tracking [Wb versus s]. Reference signal (magenta-dashed), proposed DTDFOC (black-solid), and SDFOC (gray-solid).

discussions. Again, the proposed DTIFOC is more accurate that the SIFOC.

Finally, real-time results with a sampling period of $T_s = 3000\ \mu$s are only shown for the proposed direct controller in Figs. 16 and 17. Results for the SDFOC are not shown, since the closed-loop IM was not able to be stabilized with this controller. Although both outputs are characterized by noise, it can be observed that tracking of signals for the outputs was still possible. With respect to stator currents, these no longer resemble profiles as with those with a sampling period of $T_s = 100\ \mu$s.

In the case of indirect controllers, real-time results are shown in Figs. 18 and 19. The observed accuracy in output tracking for the rotor velocity is still good, but not for the rotor flux modulus. The corresponding current profiles are characterized by noisy signals. Fig. 20 shows the real-time results for the load torque estimation in different scenarios. Since the load torque is proportional to the time derivative of the rotor velocity, an initial step is noted due to the initial ramp in the rotor velocity. In general, a more accuracy is provided by the proposed DTIFOC than the SIFOC. Output tracking results are summarized in Tables V and VI for the precision error and settling time values

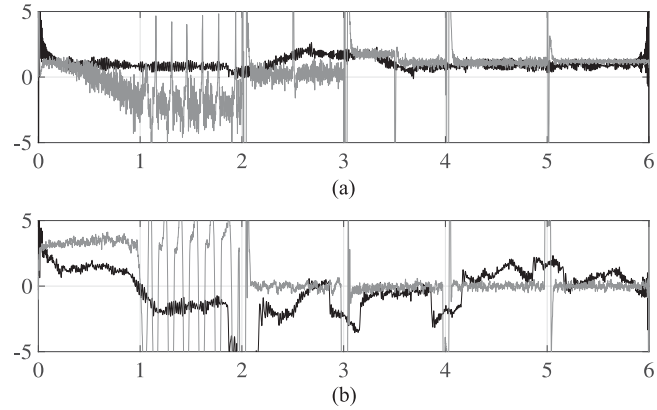

Fig. 13. Real-time stator currents components for a sampling time of $T_s = 600\ \mu$s. (a) $i_{d,k}$ [A versus s]. (b) $i_{q,k}$ [A versus s]. Proposed DTDFOC (black-solid) and SDFOC (gray-solid).

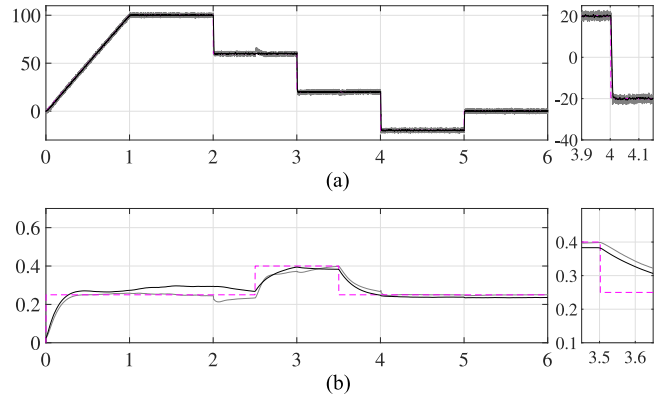

Fig. 14. Real-time output profiles implemented with a sampling time of $T_s = 600\ \mu$s. (a) Rotor velocity tracking [rad/s versus s]. (b) Rotor flux modulus tracking [Wb versus s]. Reference signal (magenta-dashed), proposed DTIFOC (black-solid), and SIFOC (gray-solid).

TABLE V
PRECISION ERROR AND SETTLING TIME EVALUATION FOR TRACKING OF THE ROTOR VELOCITY IN REAL TIME

	100 μs		600 μs		3000 μs	
	$P_e(\%)$	t_s(s)	$P_e(\%)$	t_s(s)	$P_e(\%)$	t_s(s)
DTDFOC	0.005	0.06	0.025	0.05	0.14	0.6
SDFOC	0.015	0.06	0.64	0.03	–	–
DTIFOC	0.985	0.01	0.2	0.01	0.045	0.034
SIFOC	0.18	0.02	0.97	0.02	0.515	0.03

obtained in real time. These values resemble to those obtained in simulations.

Remark 5.1: DSpace family boards are not popular in industries, but in the academic field, as can be noted from the literature. Nevertheless, it is interesting to investigate a further implementation in portable devices, such as an FPGA or an application-specific integrated circuit, where both devices are characterized by implementing algorithms in hardware. A DSP implements the algorithm in software, which is difficult to characterize due to different architectures presented by different DSPs. Given the block diagrams of the mathematical operations for performing the algorithms (the mathematical operations

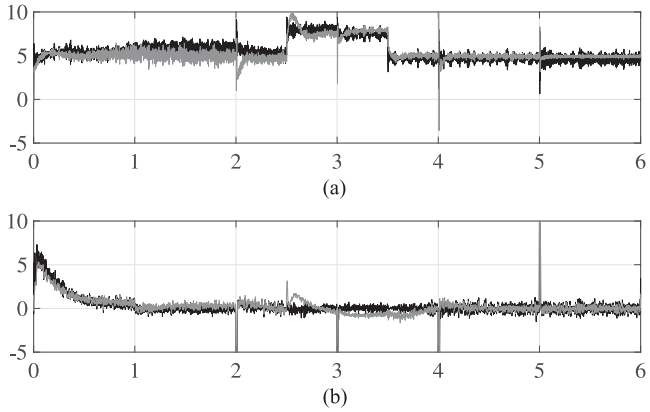

Fig. 15. Real-time stator currents components for a sampling time of $T_s = 600\ \mu$s. (a) $i_{d,k}$ [A versus s]. (b) $i_{q,k}$ [A versus s]. Proposed DTIFOC (black-solid) and SIFOC (gray-solid).

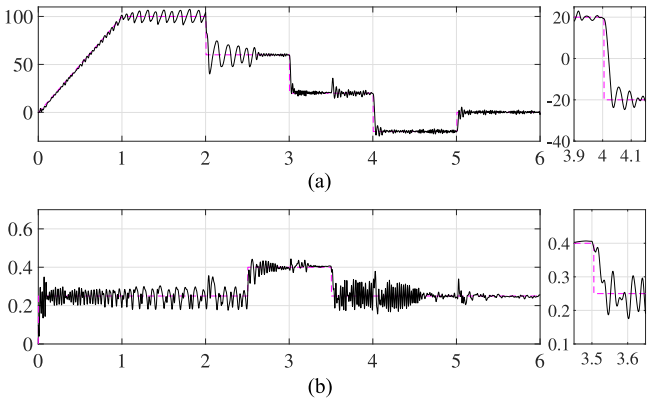

Fig. 16. Real-time output profiles implemented with a sampling time of $T_s = 3000\ \mu$s. (a) Rotor velocity tracking [rad/s versus s]. (b) Rotor flux modulus tracking [Wb versus s]. Reference signal (magenta-dashed) and proposed DTDFOC (black-solid).

TABLE VI
PRECISION ERROR AND SETTLING TIME EVALUATION FOR TRACKING OF THE ROTOR FLUX MODULUS IN REAL TIME

	100 μs		600 μs		3000 μs	
	$P_e(\%)$	t_s(s)	$P_e(\%)$	t_s(s)	$P_e(\%)$	t_s(s)
DTDFOC	0.1	0.055	0.6875	0.05	5.65	0.55
SDFOC	4.825	0.05	28.3	0.05	–	–
DTIFOC	1.625	0.5	8.8	0.5	24.1	–
SIFOC	3.95	0.5	10.65	0.5	43.8	–

for decoding the encoder signals and performing the SVPWM are not considered), the critical path [16] was determined for both proposed controllers to have a computational time $T = 2T_D + 9T_M + 9T_A + 2T_{\text{trig}} + 2T_{\text{si}}$, with T_D, T_M, and T_A being the execution times for the division, multiplication, and addition, respectively; moreover, T_{trig} and T_{si} are the execution times needed for a trigonometric function and sign inversion, respectively. Based on [31], where the latency for each operation was determined, the execution time in clock cycles for the critical path was calculated to be 311 clock cycles, and that for an

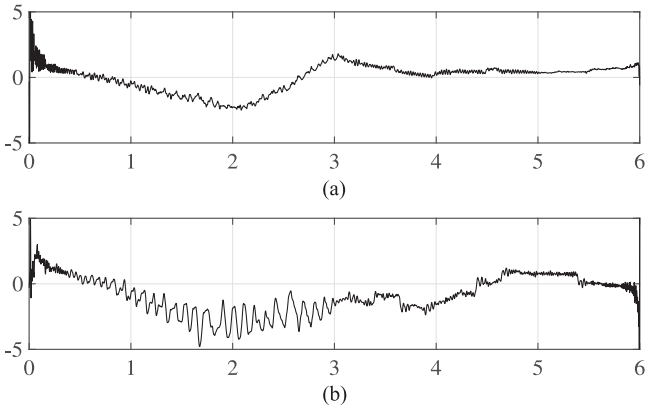

Fig. 17. Real-time stator currents components for a sampling time of $T_s = 3000\ \mu$s with the proposed DTDFOC. (a) $i_{d,k}$ [A versus s]. (b) $i_{q,k}$ [A versus s].

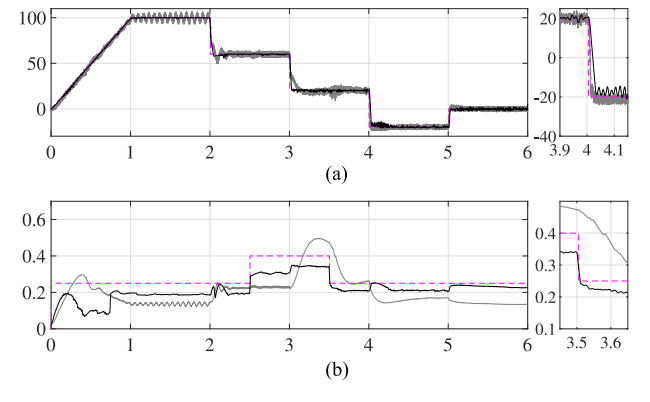

Fig. 18. Real-time output profiles implemented with a sampling time of $T_s = 3000\ \mu$s. (a) Rotor velocity tracking [rad/s versus s]. (b) Rotor flux modulus tracking [Wb versus s]. Reference signal (magenta-dashed), proposed DTIFOC (black-solid), and SIFOC (gray-solid).

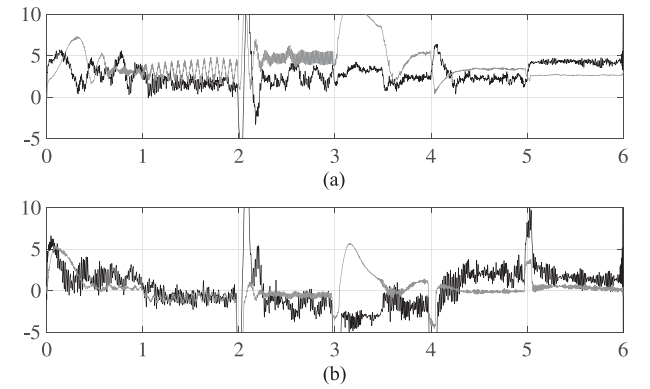

Fig. 19. Real-time stator currents components for a sampling time of $T_s = 3000\ \mu$s. (a) $i_{d,k}$ [A versus s]. (b) $i_{q,k}$ [A versus s]. Proposed DTIFOC (black-solid) and SIFOC (gray-solid).

FPGA running with a 5-MHz clock corresponds to an execution time of 62.2 μs. It is clear that in a DSP, the execution time is considerably increased due to the sequential execution of instructions. Finally, the importance of having algorithms that

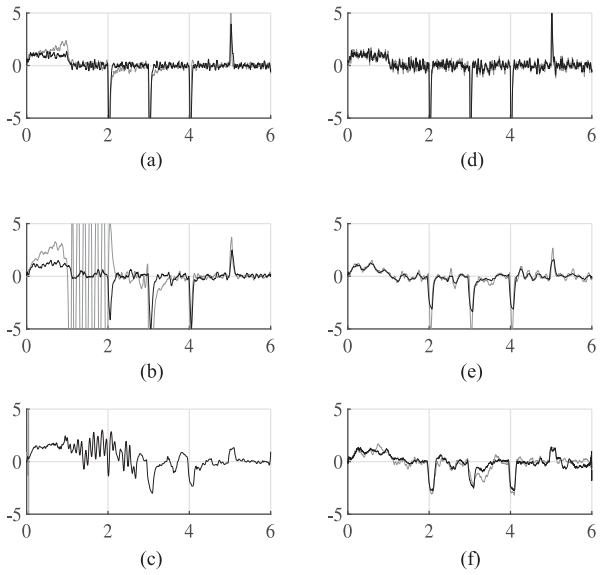

Fig. 20. Real-time load torque estimations [N· m versus s]. Direct FOCs: (a) $T_s = 100$ μs, (b) $T_s = 600$ μs, and (c) $T_s = 3000$ μs. Indirect FOCs: (d) $T_s = 100$ μs, (e) $T_s = 600$ μs, and (f) $T_s = 3000$ μs. Proposed controller (black-solid) and sampled controller (gray-solid).

can admit relatively large sampling periods that can match the computing time delay is worth mentioning.

VI. Conclusion

Controlling an IM is a challenging task due to the fact that it is a nonlinear system with time-variant parameters. Its main competitor is the dc motor with separated excitation, which, unlike the IM, is a linear system with ease of controlling it. But the FOC technique has made possible to extend the easiness of controlling dc motors to IMs; hence, FOC is a popular control technique for the IM and has become a standard in industry.

The arrival of digital technology has facilitated the implementation of controllers in digital devices; nevertheless, to get the most out of it, sampled dynamics of the system under study must be considered.

Therefore, in this article, sampled dynamics for IMs when oriented to the field was presented, and both discrete-time direct and indirect field-oriented controllers were designed in a similar fashion to the continuous-time counterpart. The easiness of designing decoupled controllers with simple PI control loops was put in evidence. With the help of numerical simulations, it was demonstrated that the IM motor performed well with both controllers even when the sampling period was increased. For comparison purposes, discretized continuous-time FOC controllers (direct and indirect) were also simulated, where the performance of the closed-loop IM starts to deteriorate when the sampling period increases. Real-time experiments were carried out in order to sustain the simulation study. With the realized experiments, a good output tracking performance was verified. In addition, the consistent relationship between the profiles for the stator currents, and rotor velocity and load torque, was put in evidence. In particular, the proposed DTIFOC yields smoother responses with respect to the proposed DTDFOC that can be attributable to the absence of a rotor flux observer.

As future work, new opportunities are recognized as follows:

1) extension of continuous-time controller techniques for IMs (sensorless, field weakening, direct torque control, etc.) to a discrete-time setting;
2) direct implementation of algorithms in digital devices;
3) possibility of using low-cost digital devices with relative low clock frequencies.

And the following new challenges are identified:

1) designing of robust or adaptive controllers for dealing with parameter variations and perturbations;
2) design of enhanced rotor or stator flux observers.

Appendix A
Stability Analysis

1) DTDFOC Stability Analysis: Let us first consider the subsystem Σ_ϕ in (9). The corresponding tracking error dynamics for $\chi_{d,k} = \phi_{d,k} - \phi_{d,r,k}$ and $e_{id,k} = i_{d,k} - i_{d,r,k}$ are as follows:

$$\chi_{d,k+1} = \eta_2 \phi_{d,k} + \eta_3 i_{d,k} - \phi_{d,r,k+1} \tag{25}$$

$$e_{id,k+1} = a_1 i_{d,k} - a_2 \phi_{d,k} - \frac{k_{12}}{\eta_3} \sum_{n=1}^{k} T_s \chi_{d,n-1} + v_{d,k} + \delta_{d,k}. \tag{26}$$

Substituting $i_{d,k} = e_{id,k} + i_{d,r,k}$ into (25), and using (12) at the same time yields

$$\begin{aligned} \chi_{d,k+1} &= k_{11}\chi_{d,k} + k_{12}\bar{g}_{d,k} + \eta_3 e_{id,k} - \phi_{d,r,k+1} \\ \bar{g}_{d,k+1} &= \bar{g}_{d,k} + T_s \chi_{d,k}. \end{aligned} \tag{27}$$

Direct substitution of (10) into (26) yields

$$\begin{aligned} e_{id,k+1} &= k_{21} e_{id,k} + k_{22} g_{d,k} + \delta_{d,k} \\ g_{d,k+1} &= g_{d,k} + T_s e_{id,k}. \end{aligned} \tag{28}$$

Combining (27) and (28) results in the following expression:

$$\xi_{d,k+1} = A_d \xi_{d,k} + D_{d,k} \tag{29}$$

where $\xi_{d,k} = (\chi_{d,k}, \bar{g}_{d,k}, e_{id,k}, g_{d,k})^T$

$$A_d = \begin{pmatrix} k_{11} & k_{12} & \eta_3 & 0 \\ T_s & 1 & 0 & 0 \\ \hline 0 & 0 & k_{21} & k_{22} \\ 0 & 0 & T_s & 1 \end{pmatrix}, \; D_{d,k} = \begin{pmatrix} -\phi_{d,r,k+1} \\ 0 \\ \hline \delta_{d,k} \\ 0 \end{pmatrix}$$

with $D_{d,k}$ being a vector of unknown constant terms. PI gains will only be illustrated for $(e_{i,d,k}, g_{d,k})^T$ subsystem. The characteristic polynomial of such a subsystem in (29) is

$$P_{cl}(z) = z^2 - (k_{21} + 1)z + (k_{21} - k_{22}T_s).$$

Then, a desired polynomial is proposed with desired poles p_1 and p_2 such that $|p_1| < 1$ and $|p_2| < 1$

$$P_d(z) = z^2 - (p_1 + p_2)z + p_1 p_2.$$

Equating the coefficients of $P_{cl}(z)$ and $P_d(z)$ yields the following explicit relations for the gains:

$$k_{21} = p_1 + p_2 - 1, \quad k_{22} = \frac{k_{21} - p_1 p_2}{T_s}.$$

In a similar fashion to the Ziegler–Nichols method, the obtained gains are used as a starting point, where the fine tuning of the gains can follow up an intuitive rule of thumb.

The partial steady-state solution $(e_{i,d,k}, g_{d,k})^T$ in (29) is $(e_{i,d,ss}, g_{d,ss})^T = (0, -\delta_{d,k}/k_{22})^T$. It is clear that the steady-state solution for the integral action $g_{d,k}$ is proportional to the unknown constant perturbation term $\delta_{d,k}$. Analyzing the dynamic equation for $e_{i,d,k}$ in steady-state results in the following expression:

$$0 = 0 + k_{22}\left(\frac{-\delta_{d,k}}{k_{22}}\right) + \delta_{d,k}$$

due to the cancelation of the unknown constant perturbation term by means of the integral action. Due to similarities among subsystems, from herein after, detailed stability analysis will be avoided for the rest of this appendix. After $e_{i,d,k} = 0$, subsystem (27) reduces to

$$\begin{aligned} \chi_{d,k+1} &= k_{11}\chi_{d,k} + k_{12}\bar{g}_{d,k} - \phi_{d,r,k+1} \\ \bar{g}_{d,k+1} &= \bar{g}_{d,k} + T_s\chi_{d,k}. \end{aligned} \tag{30}$$

The steady-state solution of (30) is $(0, -\phi_{d,r,k+1}/k_{12})^T$.

Now, let us consider the rotor velocity subsystem, where the dynamics for $\chi_{q,k}$ and $e_{iq,k}$ are as follows:

$$\begin{aligned} \chi_{q,k+1} &= \omega_k + \frac{T_s}{J}\frac{k_T}{\tau_{r,d}}\phi_{d,r,k} i_{q,k} - \frac{T_s}{J}\tau_{L,k} - \omega_{r,k+1} \\ e_{i,q,k+1} &= a_4 i_{q,k} + a_5\omega_k - \frac{k_{32}}{a_3}\sum_{n=1}^{k} T_s\chi_{q,n-1} \\ &\quad + v_{q,k} + \delta_{q,k}. \end{aligned} \tag{31}$$

Using (11) in (31) along with (13), the closed-loop rotor velocity subsystem can easily be determined as follows:

$$\begin{aligned} \chi_{q,k+1} &= k_{31}\chi_{q,k} + k_{32}\bar{g}_{q,k} + a_3 e_{iq,k} - \frac{T_s}{J}\tau_{L,k} - \omega_{r,k+1} \\ \bar{g}_{q,k+1} &= \bar{g}_{q,k} + T_s\chi_{q,k} \\ e_{iq,k+1} &= k_4 1 e_{iq,k} + k_{42} g_{q,k} + \delta_{q,k} \\ g_{q,k+1} &= g_{q,k} + T_s e_{iq,k}. \end{aligned} \tag{32}$$

The steady-state solution of (32) is $(0, T_s\tau_{L,k}/(k_{32}J), 0, -\delta_{q,k}/k_{42})^T$.

2) DTIFOC Stability Analysis: The dynamics for $e_{\phi,k}$ and for $\varepsilon_{d,k} =$ are as follows:

$$e_{\phi,k+1} = \eta_2\phi_{d,k} + \eta_3 i_{d,k} - \phi_{d,r,k+1} \tag{33}$$

$$\varepsilon_{d,k+1} = \gamma_d i_{d,k} + v_{d,k} - i_{d,r,k+1}. \tag{34}$$

Substituting (17) and (18) into (33) and (34), respectively, yields the following closed-loop rotor flux subsystem:

$$\begin{aligned} e_{\phi,k+1} &= \eta_2 e_{\phi,k} + \eta_3\varepsilon_{d,k} \\ \varepsilon_{d,k+1} &= (\gamma_d + \kappa_{11})\varepsilon_{d,k} + \kappa_{12}\zeta_{d,k} + \rho_{d,k} \\ \zeta_{d,k+1} &= \zeta_{d,k} + T_s\varepsilon_{d,k}. \end{aligned} \tag{35}$$

It is easy to determine that the steady-state solution for (35) is $(0, 0, -\rho_{d,k}/\kappa_{12})^T$.

With respect to the rotor velocity subsystem, the dynamics for $e_{\omega,k}$ and $\varepsilon_{q,k}$ are of the following form:

$$\begin{aligned} e_{\omega,k+1} &= e_{\omega,k} + \frac{T_s}{J}\tau_{e,k} - \frac{T_s}{J}\tau_{L,k} \\ \varepsilon_{q,k+1} &= \gamma_d\varepsilon_{q,k} + v_{q,k} + \gamma_d i_{q,r,k} - i_{q,r,k+1}. \end{aligned} \tag{36}$$

Substituting (21) into (36) and using (2), (19), and (20) yields the following closed-loop dynamics:

$$\begin{aligned} e_{\omega,k+1} &= (1 + \kappa_{21})e_{\omega,k} + \frac{T_s}{J}\frac{k_T}{\tau_{r,d}}\phi_{d,r,k}\varepsilon_{q,k} + \kappa_{22} g_k \\ &\quad - \frac{T_s}{J}\tau_{L,k} \\ g_{k+1} &= g_k + T_s e_{\omega,k} \\ \varepsilon_{q,k+1} &= (\gamma_d + \kappa_{31})\varepsilon_{q,k} + \kappa_{32}\zeta_{q,k} + \rho_{q,k} \\ \zeta_{q,k+1} &= \zeta_{q,k} + T_s\varepsilon_{q,k}. \end{aligned} \tag{37}$$

It can be easily determined that the vector $(\varepsilon_{q,k}, \zeta_{q,k+1})^T$ tends asymptotically to $(0, -\rho_{q,k}/\kappa_{32})^T$. Hence, the closed-loop subsystem (37) will eventually be reduced to

$$\begin{aligned} e_{\omega,k+1} &= (1 + \kappa_{21})e_{\omega,k} + \kappa_{22} g_k - \frac{T_s}{J}\tau_{L,k} \\ g_{k+1} &= g_k + T_s e_{\omega,k}. \end{aligned} \tag{38}$$

In a similar fashion, vector $(e_{\omega,k}, g_k)^T$ in (38) asymptotically tends to $(0, T_s\tau_{L,k}/(J\kappa_{22}))^T$, accomplishing the tracking of a desired reference signal $\omega_{r,k}$ for the rotor velocity ω_k.

APPENDIX B
SAMPLED VERSION OF FOCS

Both controllers, DFOC and IFOC, cancel out the old dynamics of the stator currents and introduce the new dynamics through the sampled variables $v_{d,k}$ and $v_{q,k}$ as follows:

$$\begin{aligned} u_{d,k} &= \sigma\left(-p\omega_k i_{q,k} - \frac{L_m i_{q,k}^2}{\tau_r\phi_{d,k}} - \frac{\beta}{\tau_r}\phi_{d,k} + v_{d,k}\right) \\ u_{q,k} &= \sigma\left(p\omega_k i_{d,k} + \frac{L_m i_{q,k} i_{d,k}}{\tau_r\phi_{d,k}} + \beta p\omega_k\phi_{d,k} + v_{q,k}\right). \end{aligned} \tag{39}$$

It is clear that controls in (39) have the same purposes of those described for (7). In what follows, all the integral actions (41), (43), and (51) are approximations obtained by means of the explicit Euler method.

1) Sampled DFOC: Given $\phi_{d,r,k}$, the reference signal for the stator d component results as follows:

$$\begin{aligned} i_{d,r,k} &= \frac{\tau_r}{L_m}\left(-p_{d,1}(\phi_{d,k} - \phi_{d,r,k}) - p_{d,2}\zeta_{d,k}\right) \\ i_{q,r,k} &= \frac{J}{k_T\phi_{d,r,k}}\left(-p_{q,1}(\omega_k - \omega_{r,k}) - p_{q,2}\zeta_{q,k}\right) \end{aligned} \tag{40}$$

where $\zeta_{d,k}$ and $\zeta_{q,k}$ in (40) are integral actions defined as

$$\begin{aligned}\zeta_{d,k+1} &= \zeta_{d,k} + T_s(\phi_{d,k} - \phi_{d,r,k})\\ \zeta_{q,k+1} &= \zeta_{q,k} + T_s(\omega_k - \omega_{r,k}).\end{aligned} \tag{41}$$

The control inputs $v_{d,k}$ and $v_{q,k}$ are proposed as PI control loops

$$\begin{aligned}v_{d,k} &= -\bar{p}_{d,1}(i_{d,k} - i_{d,r,k}) - \bar{p}_{d,2}\bar{\zeta}_{d,k} - \varphi_{d,k}\\ v_{q,k} &= -\bar{p}_{q,1}(i_{q,k} - i_{q,r,k}) - \bar{p}_{q,2}\bar{\zeta}_{q,k} - \varphi_{q,k}\end{aligned} \tag{42}$$

where $\bar{\zeta}_{d,k}$ and $\bar{\zeta}_{q,k}$ in (42) are the integral actions with the following dynamics:

$$\begin{aligned}\bar{\zeta}_{d,k+1} &= \bar{\zeta}_{d,k} + T_s(i_{d,k} - i_{d,r,k})\\ \bar{\zeta}_{q,k+1} &= \bar{\zeta}_{q,k} + T_s(i_{q,k} - i_{q,r,k}).\end{aligned} \tag{43}$$

The functions $\varphi_{d,k}$ and $\varphi_{q,k}$ account for the old dynamics

$$\begin{aligned}\varphi_{d,k} &= -\gamma i_{d,k} - \dot{i}_{d,k}\\ \varphi_{q,k} &= -\gamma i_{q,k} - \dot{i}_{q,k}.\end{aligned} \tag{44}$$

Functions (44) can be omitted for the sake of simplicity of the control inputs; in such a case, the integral actions (43) can attenuate them.

The rotor position is estimated with rotor flux components in the stationary reference frame

$$\hat{\theta}_{\phi,k} = a\tan(\hat{\phi}_{\beta,k}/\hat{\phi}_{\alpha,k}) \tag{45}$$

with

$$\hat{\phi}_{r,k+1} = \hat{\phi}_{r,k} - \frac{T_s}{\tau_r}\hat{\phi}_k + p\omega_k\mathcal{J}\hat{\phi}_k + \frac{L_m T_s}{\tau_r}I_{s,k} \tag{46}$$

where $\hat{\phi}_{r,k} = (\hat{\phi}_{\alpha,k}, \hat{\phi}_{\beta,k})^T$. Estimations in (45) and (46) are similar to those in (15) and (14), respectively.

2) Sampled IFOC: With $\phi_{d,r,k}$ available, the reference signal for the d current component is proposed as

$$i_{d,r,k} = \frac{\phi_{d,r,k}}{L_m}. \tag{47}$$

It can be verified that (47) corresponds exactly to (17). The electromagnetic torque can be considered as a pseudoinput in the mechanical equation, where a reference signal can be proposed as

$$\begin{aligned}\tau_{e,r,k} &= -Jc_1(\omega_k - \omega_{r,k}) - Jc_2 z_k\\ z_{k+1} &= z_k + T_s(\omega_k - \omega_{r,k})\end{aligned} \tag{48}$$

where z_k is an integral action. Once $\phi_{d,r,k}$ and (48) are available, the reference signal for the q current component is proposed as

$$i_{q,r,k} = \frac{\tau_{e,r,k}}{k_T\phi_{d,r,k}}. \tag{49}$$

When $T_s = 0$, (20) yields exactly to (49). The fictitious control inputs $v_{d,k}$ and $v_{q,k}$ are proposed as single current control loops

$$\begin{aligned}v_{d,k} &= -c_{d,1}(i_{d,k} - i_{d,r,k}) - c_{d,2}z_{d,k}\\ v_{q,k} &= -c_{q,1}(i_{q,k} - i_{q,r,k}) - c_{q,2}z_{q,k}\end{aligned} \tag{50}$$

where the integrators $z_{d,k}$ and $z_{q,k}$ are defined as

$$\begin{aligned}z_{d,k+1} &= z_{d,k} + T_s(i_{d,k} - i_{d,r,k})\\ z_{q,k+1} &= z_{q,k} + T_s(i_{q,k} - i_{q,r,k}).\end{aligned} \tag{51}$$

Finally, the rotor angular position is calculated as

$$\theta_{\phi,k+1} = \theta_{\phi,k} + T_s\left(p\omega_k + \frac{L_m i_{q,r,k}}{\tau_r\phi_{d,r,k}}\right). \tag{52}$$

The similarities between (52) and (23) can be noted.

REFERENCES

[1] F. Blaschke, "The principle of field orientation as applied to the new transvector closed-loop control system for rotating field machines," *Siemens Rev.*, vol. 39, no. 5, pp. 217–220, 1972.

[2] S. M. Tripathi and R. Vaish, "Taxonomic research survey on vector controlled induction motor drives," *IET Power Electron.*, vol. 12, no. 7, pp. 1603–1615, 2019.

[3] Z. Yin, C. Du, J. Liu, X. Sun, and Y. Zhong, "Research on autodisturbance-rejection control of induction motors based on an ant colony optimization algorithm," *IEEE Trans. Ind. Electron.*, vol. 65, no. 4, pp. 3077–3094, Apr. 2018.

[4] J. N. Forestieri, M. Farasat, and A. M. Trzynadlowski, "Indirect real- and reactive-power control of induction motor drives," *IEEE J. Emerg. Sel. Topics Power Electron.*, vol. 6, no. 4, pp. 2109–2125, Dec. 2018.

[5] M. Fateh and R. Abdellatif, "Comparative study of integral and classical backstepping controllers in IFOC of induction motor fed by voltage source inverter," *Int. J. Hydrogen Energy*, vol. 42, no. 28, pp. 17953–17964, 2017.

[6] A. Ammar, A. Bourek, and A. Benakcha, "Nonlinear SVM-DTC for induction motor drive using input-output feedback linearization and high order sliding mode control," *ISA Trans.*, vol. 67, pp. 428–442, 2017.

[7] C. Cruz, M. A. Gallegos, R. Alvarez, and F. Pazos, "Comparison of several nonlinear controllers for induction motors," in *Proc. 9th IEEE Int. Power Electron. Congr.*, 2004, pp. 134–139.

[8] H. Rehman and R. Dhaouadi, "A fuzzy learning-sliding mode controller for direct field-oriented induction machines," *Neurocomputing*, vol. 71, nos. 13–15, pp. 2693–2701, 2008.

[9] F. Alonge, M. Cirrincione, F. D'Ippolito, M. Pucci, and A. Sferlazza, "Robust active disturbance rejection control of induction motor systems based on additional sliding-mode component," *IEEE Trans. Ind. Electron.*, vol. 64, no. 7, pp. 5608–5621, Jul. 2017.

[10] J. Travieso-Torres and M. Duarte-Mermoud, "Two simple and novel SISO controllers for induction motors based on adaptive passivity," *ISA Trans.*, vol. 47, no. 1, pp. 60–79, 2008.

[11] S. Gdaim, A. Mtibaa, and M. F. Mimouni, "Design and experimental implementation of DTC of an induction machine based on fuzzy logic control on FPGA," *IEEE Trans. Fuzzy Syst.*, vol. 23, no. 3, pp. 644–655, Jun. 2015.

[12] S. Padmanaban *et al.*, "Wavelet-fuzzy speed indirect field oriented controller for three-phase AC motor drive—Investigation and implementation," *Eng. Sci. Technol., Int. J.*, vol. 19, no. 3, pp. 1099–1107, 2016.

[13] M. Tousizadeh, M. Ojaghi, H. S. Che, J. Selvaraj, N. A. Rahim, and B. Ooi, "Fault-tolerant field-oriented control of three-phase induction motor based on unified feedforward method," *IEEE Trans. Power Electron.*, vol. 34, no. 8, pp. 7172–7183, Aug. 2019.

[14] D. Efimov, A. Polyakov, A. Levant, and W. Perruquetti, "Realization and discretization of asymptotically stable homogeneous systems," *IEEE Trans. Autom. Control*, vol. 62, no. 11, pp. 5962–5969, Nov. 2017.

[15] X. Chengi, R. Song, G. Xie, Y. Zhang, and Y. Zhang, "A new FPGA-based segmented delay-line DPWM with compensation for critical path delays," *IEEE Trans. Power Electron.*, vol. 33, no. 12, pp. 10794–10802, Dec. 2018.

[16] K. K. Parhi, *VLSI Digital Signal Processing Systems*. New York, NY, USA: Wiley, 1999.

[17] A. N. Guzmán, S. Di Gennaro, J. Rivera Domínguez, C. Acosta, A. Loukianov, and B. C.-Toledo, "Enhanced discrete-time modeling via variational integrators and digital controller design for ground vehicles," *IEEE Trans. Ind. Electron.*, vol. 63, no. 10, pp. 6375–6385, Oct. 2016.

[18] R. Ortega and D. Taoutaou, "A globally stable discrete-time controller for current-fed induction motors," *Syst. Control Lett.*, vol. 28, no. 3, pp. 123–128, 1996.

[19] M. Petronijević, B. P.-Draženović, Č. Milosavljavić, and S. R. Veselić, "Discrete-time speed servo system design—A comparative study: Proportional–integral versus integral sliding mode control," *IET Control Theory Appl.*, vol. 11, no. 16, pp. 2671–2679, 2017.
[20] B. Veselić, B. P.–Draženović, and Č. Milosavljević, "Improved discrete-time sliding-mode position control using Euler velocity estimation," *IEEE Trans. Ind. Electron.*, vol. 57, no. 11, pp. 3840–3847, Dec. 2010.
[21] A. Proca, A. Keyhani, V. Utkin, and J. Miller, "Discrete time sliding mode, continuous time sliding mode and vector control of induction motors," *Int. J. Control*, vol. 75, no. 12, pp. 901–909, 2002.
[22] R. P. Vieira, C. C. Gastaldini, R. Z. Azzolin, and H. A. Grundling, "Discrete-time sliding mode speed observer for sensorless control of induction motor drives," *IET Electr. Power Appl.*, vol. 6, no. 9, pp. 681–688, 2012.
[23] E. Q.-Manriquez, E. N. Sanchez, R. G. Harley, S. Li, and R. A. Felix, "Neural inverse optimal control implementation for induction motors via rapid control prototyping," *IEEE Trans. Power Electron.*, vol. 34, no. 6, pp. 5981–5992, Jun. 2019.
[24] I. E. Dueñas, J. Rivera, and S. S. O. Di Gennaro, "Discrete-time field oriented control for induction motors," *IFAC-PapersOnLine*, vol. 50, no. 1, pp. 15760–15765, 2017.
[25] J. Rivera, "Discrete-time modeling and control of induction motors by means of variational integrators and sliding modes—Part I: Mathematical modeling," *IEEE Trans. Ind. Electron.*, vol. 62, no. 9, pp. 5393–5401, Sep. 2015.
[26] J. Rivera, "Discrete–time modeling and control of induction motors by means of variational integrators and sliding modes—Part II: Control design," *IEEE Trans. Ind. Electron.*, vol. 62, no. 10, pp. 6183–6193, Oct. 2015.
[27] G. R.-Astorga, J. D. S.-Torres, J. Cañedo, and A. G. Loukianov, "High-order sliding mode block control of single-phase induction motor," *IEEE Trans. Control Syst. Technol.*, vol. 22, no. 5, pp. 1828–1836, Sep. 2014.
[28] K. J. Åström and T. Hägglund, *PID Controllers*. Research Triangle Park, NC, USA: Int. Soc. Meas. Control, 1995.
[29] Q. Xiao, F. Tang, Z. Xin, J. Zhou, P. Chen, and P. Chian, "Large time-delay decoupling and correction in synchronous complex-vector frame," *IET Power Electron.*, vol. 12, no. 2, pp. 254–266, 2019.
[30] V. Utkin, "Discussion aspects of high-order sliding mode control," *IEEE Trans. Autom. Control*, vol. 61, no. 3, pp. 829–833, Mar. 2016.
[31] C. Acosta, S. Di Gennaro, A. Navarrete, S. O.-Cisneros, and J. Rivera, "Digital implementation via FPGA of controllers for active control of ground vehicles," *IEEE Trans. Ind. Inform.*, vol. 15, no. 4, pp. 2253–2264, Apr. 2019.

Jorge Rivera Domínguez was born in El Rosario, México, in 1975. He received the B.Sc. degree from the Technological Institute of the Sea, Mazatlán, México, in 1999, and the M.Sc. and Ph.D. degrees in electrical engineering from the Advanced Studies and Research Center (CINVESTAV), National Polytechnic Institute (IPN), Guadalajara, México, in 2001 and 2005, respectively.

Since 2006, he has been a Full-Time Professor with the Department of Electronics, Universidad de Guadalajara, Guadalajara. He is currently commissioned as a CONACyT professorship to the CINVESTAV, IPN, Guadalajara Campus. He has authored or coauthored more than 60 technical papers and has served as reviewer for different international journals and conferences. His research interests include regulator theory, sliding-mode control, discrete-time nonlinear control systems, their applications to electrical machines, and their implementations in reconfigurable digital devices.

Iván Dueñas received the B.Sc. degree in electronic engineering from the University of Guadalajara, Guadalajara, México, in 2013, and the M.Sc. degree in electrical engineering in 2015 from the Advanced Studies and Research Center, National Polytechnic Institute, Guadalajara, where he is currently working toward the Ph.D. degree in electrical engineering with the Advanced Studies and Research Center, National Polytechnic Institute.

Susana Ortega-Cisneros received the B.S. degree in communications and electronics from the University of Guadalajara, Guadalajara, México, in 1990, the master's degree from the Center of Research and Advanced Studies, Zacatenco IPN, México City, México, in 1995, and the Ph.D. degree in computer science and telecommunications from the Autonomous University of Madrid, Madrid, Spain, in 2005.

She is involved in the design of digital architectures based on field-programmable gate arrays (FPGAs), digital signal processors (DSPs), and microprocessors. Her current research interests include digital control, self-timed synchronization, electronic systems applied to biomedicine, embedded microprocessor design, digital electronics, and custom DSPs in FPGAs.